

Topological phase transition in compressed van der Waals superlattice heterostructure $BiTeCl/HfTe_2$

Zhilei Li(李志磊), Yinxiang Li(李殷翔), Yiting Wang(王奕婷), Wenzhi Chen(陈文执), and Bin Chen(陈斌)
Citation: Chin. Phys. B, 2024, 33 (**8**): 087102. DOI: 10.1088/1674-1056/ad462e

What follows is a list of articles you may be interested in

Two-dimensional Sb net generated nontrivial topological states in $SmAgSb_2$ probed by quantum oscillations

Jian Yuan(袁健), Xian-Biao Shi(石贤彪), Hong Du(杜红), Tian Li(李田), Chuan-Ying Xi(郗传英), Xia Wang(王霞), Wei Xia(夏威), Bao-Tian Wang(王保田), Rui-Dan Zhong(钟瑞丹), and Yan-Feng Guo(郭艳峰)
Chin. Phys. B, 2024, 33 (**7**): 077102. DOI: 10.1088/1674-1056/ad4bc2

Spin direction dependent quantum anomalous Hall effect in two-dimensional ferromagnetic materials

Yu-Xian Yang(杨宇贤) and Chang-Wen Zhang(张昌文)
Chin. Phys. B, 2024, 33 (**4**): 047101. DOI: 10.1088/1674-1056/ad1380

Design of sign-reversible Berry phase effect in 2D magneto-valley material

Yue-Tong Han(韩曰通), Yu-Xian Yang(杨宇贤), Ping Li(李萍), and Chang-Wen Zhang(张昌文)
Chin. Phys. B, 2023, 32 (**9**): 097101. DOI: 10.1088/1674-1056/acd920

Topological properties of tetratomic Su-Schrieffer-Heeger chains with hierarchical long-range hopping

Guan-Qiang Li(李冠强), Bo-Han Wang(王博涵), Jing-Yu Tang(唐劲羽), Ping Peng(彭娉), and Liang-Wei Dong(董亮伟)
Chin. Phys. B, 2023, 32 (**7**): 077102. DOI: 10.1088/1674-1056/aca7ef

SU(3) spin-orbit coupled fermions in an optical lattice

Xiaofan Zhou(周晓凡), Gang Chen(陈刚), and Suo-Tang Jia(贾锁堂)
Chin. Phys. B, 2022, 31 (**1**): 017102. DOI: 10.1088/1674-1056/ac11dc

---

Topological phase transition in compressed van der Waals superlattice heterostructure BiTeCl/$HfTe_2$

Zhilei Li(李志磊), Yinxiang Li(李殷翔)†, Yiting Wang(王奕婷), Wenzhi Chen(陈文执), and Bin Chen(陈斌)

Tin Ka-Ping College of Science, University of Shanghai for Science and Technology, Shanghai 200093, *China*

(Received 6 February 2024; revised manuscript received 21 April 2024; accepted manuscript online 2 May 2024)

Based on first-principles calculations, we investigate the electronic band structures and topological properties of heterostructure BiTeCl/$HfTe_2$ under c-direction strain. In the primitive structure, this material undergoes a phase transition from an insulator with a narrow indirect gap to a metal by strong spin–orbital coupling. When strain effect is considered, band inversion at time-reversal invariant point Z is responsible for the topological phase transition. These nontrivial topologies are caused by two different types of band crossings. The observable topological surface states in (110) surface also support that this material experiences topological phase transition twice. The layered heterostructure with van der Waals force provides us with a new desirable platform upon which to control topological phase transition and construct topological superconductors.

Keywords: topological phase transition, surface states, strain effect, heterostructure

PACS: 71.15.Mb, 71.30.+h, 73.20.At, 74.78.Fk **DOI:** 10.1088/1674-1056/ad462e

1. Introduction

In recent decades, topology and superconductivity have been the most active research fields in condensed matter physics. Various novel topological states are found in theoretical calculations and experiments, such as three-dimensional (3D) topological insulators,[1,2] Dirac semimetals,[3–7] Weyl semimetals,[8,9] nodal-ring semimetals[10] and higher-order topological insulators.[11] Meanwhile, the underlying mechanisms of high-transition-temperature superconductivity in cuprates and iron-based compounds are still elusive. Recently, nickelate compound $La_3Ni_2O_7$ was found to show the signature of superconductivity near 80 K under high pressure.[12] The topological states in high-temperature superconductors can be used to realize Majorana fermions for topological quantum computation.[13,14] Based on the proximity effect in heterostructures, the interface between topological insulators and s-wave superconductors can host helical topological surface states.[15] The proposed superconducting units are intercalated into topological insulators and form a strategy to search for topological superconductivity.[16] Interfacial superconductors offer a new route towards tunable superconductivity by chemical doping and electric field gating.[17] Hence, the natural combination of topology and superconductivity in layered heterostructures has advantages in terms of realizing topological superconductors.

Layered noncentrosymmetric bismuth tellurohalides with large Rashba spin–orbital coupling (SOC) are potential materials for spintronic devices.[18,19] The topological insulating state and superconducting phase are found in Rashba semimetal BiTeCl under high pressure.[20] Moreover, various novel properties have been proposed in monolayer transition metal dichalcogenide $HfTe_2$, such as Dirac semimetal, charge density wave and Ising superconductivity.[22,23] Strong SOC in two-dimensional (2D) materials may lead to Ising superconductivity.[24] The heterostructure of intercalated layers BiTeCl and $HfTe_2$ provides us with a chance to search for nontrivial topology and interfacial superconductivity. The topology-protected surface states can be directly observed by angle-resolved photoemission spectroscopy (ARPES). The coexistence of topological surface state and superconductivity may be realized in this intercalated layer material by electron doping. In nontrivial topological materials, Majorana-bound states can also be tested in vortex cores using scanning tunneling microscopy.

In this paper, the topological properties of heterostructure BiTeCl/$HfTe_2$ under c-direction strain are studied by first-principles calculations. In the primitive structure, strong SOC in heavy Hf, Bi and Te atoms leads to a phase transition from an insulator with a narrow energy gap to metal. In order to obtain observable topological surface states, we calculate electronic band structures of this heterostructure with three different strengths of c-direction strain. In the $\Delta c/c = -0.0822$ case, the band inversion between the p_z orbital of atoms (Te1, Bi) and the (p_x, p_y) orbitals of atom Te2 at time-reversal invariant point (TRIP) Z results is topologically nontrivial. This topological property is supported by a Dirac cone located at $\widetilde{Z}$ above Fermi level 0.15 eV on a (110) surface. In the $\Delta c/c = -0.1233$ case, vanishing of band inversion occurs, which is accompanied by disappearance of the Dirac cone. In

†Corresponding author. E-mail: yinxiangl@hotmail.com

© 2024 Chinese Physical Society and IOP Publishing Ltd

$\Delta c/c = -0.1644$ case, the p_z orbital of atoms (Te1, Te2), the p_y orbital of Te1 atoms and the p_z orbital of Bi atoms are responsible for this band crossing. The corresponding topological surface state is above the Fermi level 0.25 eV on the (110) surface. Thus, topological phase transitions take place twice in layered heterostructure BiTeCl/$HfTe_2$ with van der Waals force.

The paper is organized as follows. In Section 2, we mainly illustrate the crystal structure of layered heterostructure BiTeCl/$HfTe_2$. The primary parameter settings for first-principles calculations are listed in this section. In Section 3, we present the electronic band structures and density of states (DOS) of this heterostructure. Under three different strengths of strain, we calculate corresponding electronic band structures and surface states of this material. In Section 4, we summarize the main properties of electronic band structures in layered heterostructure BiTeCl/$HfTe_2$ under c-direction strain. These results provide more useful information to search for layered topological materials and topological superconductors.

2. Crystal structure and method

The ternary compound BiTeCl is a noncentrosymmetric layered material that exhibits superconductivity at pressure above 13 GPa.[20] This material belongs to hexagonal space group $P6_3mc$ (No. 186) with lattice parameters $a = b = 4.2837$ Å and $c = 13.0904$ Å. Each monolayer is composed of a Te–Bi–Cl sandwich structure; hence the material is also referred to as a Janus crystal.[25] The layers are connected by van der Waals force and are staggered to form a unit cell. Numerous novel physical effects have been observed experimentally in this material, such as the Rashba effect, topological states and superconductivity.[20,26] Meanwhile, the binary compound $HfTe_2$ is a transition-metal dichalcogenides material with inversion symmetry. The corresponding lattice parameters are $a = b = 3.9924$ Å and $c = 7.0324$ Å with space group $P\bar{3}m1$ (No. 164). Theoretical calculations indicated that Ising superconductors and charge density waves (CDWs) can be realized in monolayer 1T-$HfTe_2$.[22]

In order to search for topological superconductors, we constructed a heterostructure using these two kinds of layered material, namely BiTeCl and $HfTe_2$. This assembly strategy, underpinned by experimental evidence,[31–34] is aimed at facilitating the exploration of topological surface states. The heterostructure BiTeCl/$HfTe_2$ is composed of single-layer BiTeCl and $HfTe_2$ stacked alternately along the c-direction. Based on different stacking methods and relative positions, we have considered six possible stacking methods for the 1×1 original lattice, named AB-1, AB-2, AB-3, AA-1, AA-2 and AA-3. The stacking mode of the AB structure is an asymmetric interlayer arrangement, in which the atoms of adjacent layers are completely misaligned. The structure of AB-1 is shown in Fig. 1(a). The structures of AB-2 and AB-3 are obtained by translating 1/3 and 2/3 of the lattice on the basis of AB-1. AA stacking refers to the precise or partial alignment of adjacent layers of atoms in the c-direction. Among them, AA-1 is obtained by aligning the Te atoms in $HfTe_2$ with the Te atoms in BiTeCl, AA-2 is obtained by aligning the Te atoms in $HfTe_2$ with the Cl atoms in BiTeCl, and AA-3 is obtained by aligning the two Te atoms in $HfTe_2$ with the Te and Cl atoms in BiTeCl, respectively. Relaxation calculations are performed on six different structures and their total energies without entropy are compared. It has been found that the van der Waals heterostructure of the AB-1 structure (space group $P3m1$, No. 156) is the lowest energy state. The lattice parameters, total system energy and binding energy after relaxation are shown in Table 1. The lattice parameters of AB-1 are $a = b = 4.1296$ Å, $c = 14.6074$ Å. The lattice mismatch rate of the heterostructure is 6.8%. There are two types of Te atoms in the heterostructure BiTeCl/$HfTe_2$. The Te atom in BiTeCl is called Te1, while the other in material $HfTe_2$ is called Te2. The related 3D Brillouin zone (BZ) along the high-symmetry paths for calculations is displaced in Fig. 1(b). The red solid lines represent the paths used for electronic band calculations.

Table 1. Lattice constant, without entropy total energy (E) and binding energy (E_b) of the BiTeCl/$HfTe_2$ heterostructure with different structures after relaxation.

	a (Å)	c (Å)	E (eV)	E_b (meV/Å^2)
AB-1	4.1296	14.6074	–31.1100	–3.10
AB-2	4.1304	14.5058	–31.1084	–2.98
AB-3	4.1277	14.5217	–31.1073	–2.91
AA-1	4.1281	15.4854	–31.0967	–2.27
AA-2	4.1278	15.3402	–31.1009	–2.51
AA-3	4.1298	17.0577	–31.0831	–1.49

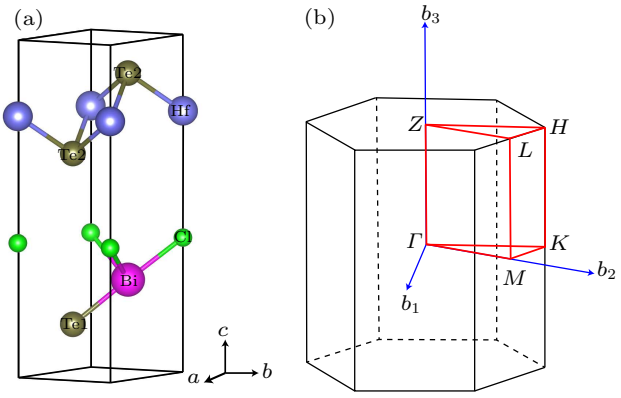


Fig. 1. (a) The primitive crystal structure of heterostructure BiTeCl/$HfTe_2$. (b) The red solid lines represent high-symmetry paths in the BZ of this heterostructure.

Based on first-principles calculations, we study the electronic band structures of heterostructure BiTeCl/$HfTe_2$ by us-

ing the projector augmented wave (PAW) method encoded in the Vienna *ab initio* simulation package (VASP).[27–29] For exchange–correlation potential, we adopt the generalized gradient approximation (GGA) of Perdew–Burke–Ernzerhof (PBE) type.[36] Electron–ion interactions are represented through PAW potential, while a plane-wave basis set with 550 eV energy cutoff was utilized. The Monkhorst–Pack[37] scheme for BZ sampling in reciprocal space uses an $11\times11\times3$ k-point mesh. Based on Green's function for a semi-infinite system, the surface states on the projected 2D BZ are studied by fitting bands near the Fermi level. By using Z2Pack codes,[38] the topological invariants are used to check the topological properties in normal states.

3. Calculation and result

In order to study the topological properties of heterostructure BiTeCl/$HfTe_2$, we investigated the electronic band structures and DOS of this material by using first-principles calculations, as shown in Fig. 2. When SOC is not considered, this material is an insulator with a narrow indirect energy gap of 0.12 eV, while the direct energy gap exceeds 0.7 eV. The energy gap near the Fermi level is contributed by d orbitals of atom Hf and p orbitals of atom Te2 respectively. This phenomenon can be verified by the result of the DOS calculation in Fig. 2(c). The main components of the conduction and valence bands are d orbitals of atom Hf and p orbitals of atom Te2 separately.

In the SOC case, the material has undergone phase transition from an insulator with a narrow indirect gap to metal. The conduction bands are pulled down at high-symmetry points (M, L), while valence bands are lifted up at high-symmetry points (Γ, Z). Thus, hole pockets and electron pockets near the Fermi level are contributed mainly by d orbitals of atom Hf and p orbitals of atom Te2 individually. The direct energy gap along Γ–Z is closed up by the p orbitals of atoms Bi and Te1 and p orbitals of atom Te2. The heavy strength of SOC in atoms Bi and Te is responsible for this transition. In order to illustrate the band crossing at Γ and Z clearly, detailed the electronic band structure is shown in inset of Fig. 2(b). We have not found any observable topological surface states through our theoretical analysis and calculations. The band transition from insulator to metal is consistent with the DOS result, which shows that the closing of energy gap is caused by the d orbitals of atom Hf in Fig. 2(d). Meanwhile, the components of the p orbitals of atoms Bi and Te1 above the Fermi level are increased significantly.

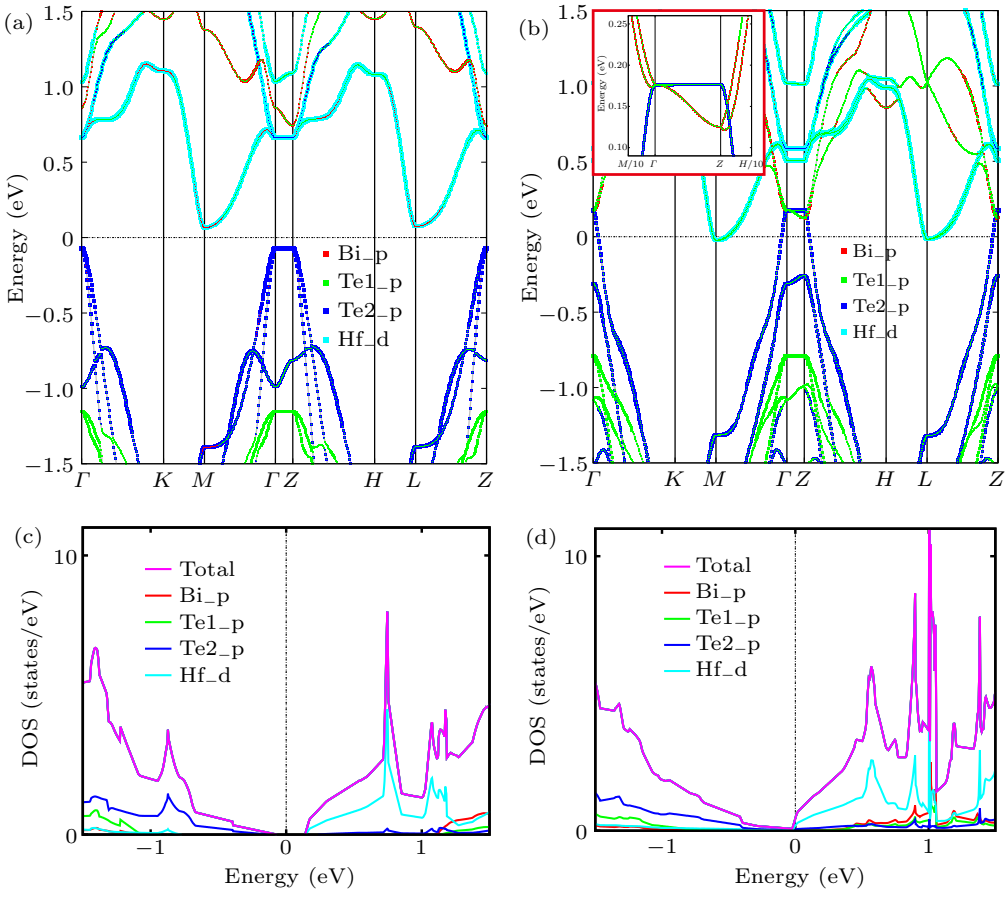


Fig. 2. Electronic band structures of heterostructure BiTeCl/$HfTe_2$ (a) without and (b) with SOC along high-symmetry paths of the BZ. Inset of (b) is the detailed band structure with SOC near the Fermi level along Γ–Z. The corresponding partial density of states of heterostructure BiTeCl/$HfTe_2$ without and with SOC are shown in (c) and (d), respectively.

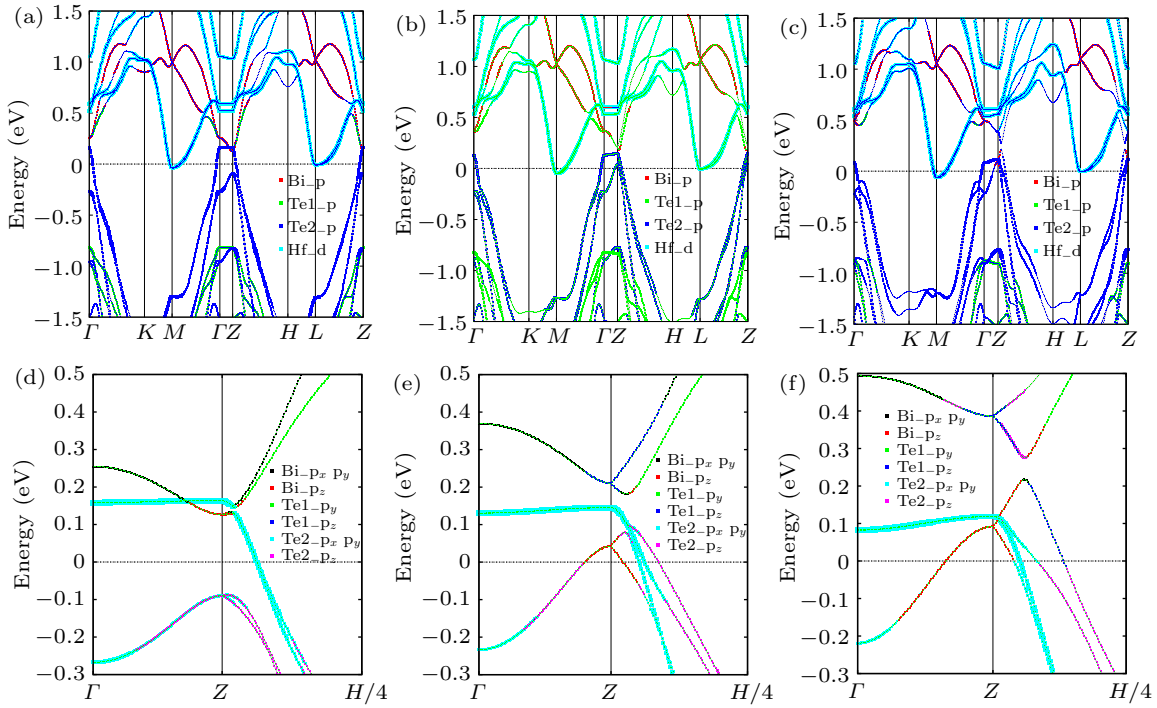


Fig. 3. Electronic band structures of heterostructure BiTeCl/$HfTe_2$ with SOC at compressed lattice parameters 1.2 Å ($\Delta c/c = -0.0822$), 1.8 Å ($\Delta c/c = -0.1233$) and 2.4 Å ($\Delta c/c = -0.1644$) are shown in (a), (b) and (c), respectively. The detailed band structures near the Fermi level along Γ–Z–$H/4$ are shown in (d), (e) and (f).

In order to search for observable topological surface states and topological superconductivity, we consider the strain effect in the c-direction on this heterostructure with van der Waals force. First, the strain effect on the electronic band structure of heterostructure BiTeCl/$HfTe_2$ with a compressed lattice parameter 1.2 Å ($\Delta c/c = -0.0822$) is displayed in Fig. 3(a). Due to weak coupling of van der Waals material in the c-direction, band structures near the Fermi level were not found to have obvious variations along the high-symmetry paths in planes $k_z = 0$ and $k_z = \pi$. The main changes are concentrated near the Γ–Z path, which is the result of applying strain along the c-direction.[39] In the Γ–Z-direction, the slope of the energy band represents the group velocity of electrons in the c-direction of real space. When it is compressed, the connections between layers along the c-direction become closer, and the adjacency effect becomes stronger, which leads to an increase in the slope of the energy band along the Γ–Z direction. The p_z orbitals of all atoms respond significantly to strain, while the responses of the (p_x, p_y) orbitals are much smaller. The spectral band on Γ–Z is contributed by the p orbitals of atoms Bi and Te1. When compressed, due to the significant increase in the absolute value of the slope of band I (bands I–VII as shown in Figs. 3(d)–3(f)), while band II remains almost unchanged, band I and band II inversion occurs between Γ–Z. This movement leads to band inversion in TRIP Z, which is the reason for the nontrivial topology. To illustrate the contribution of orbitals, the details of band inversion are shown in Fig. 3(d). The band crossing along Γ–Z is contributed by p orbitals of atom Bi and (p_x, p_y) orbitals of atom Te2, which has not been opened up by the SOC effect. This crossing means that topological semimetal phase may be realized in the material. The band crossings along Z–H between the p_z orbitals of atoms (Te1, Bi) and (p_x, p_y) orbitals of atom Te2 are opened weakly. The small energy gap with 15 meV along the Z–H-direction enables us to observe possible topological surface states on the (110) surface.

Second, we increase the strain effect along the c-direction on this heterostructure BiTeCl/$HfTe_2$ with compressed lattice parameter 1.8 Å ($\Delta c/c = -0.1233$). In Fig. 3(b), d orbitals of atom Hf are pulled down to enlarge the electron pocket at M, while p orbitals of atom Te2 are lifted up to form an additional hole pocket at Z. The bands along the Γ–Z path are primarily contributed by the p orbitals of atoms Bi and Te1. Upon compression, band I continues to rise, while band II remains almost constant. This motion causes the band inversion between path Γ–Z to disappear. The band inversion of TRIP Z disappears and this leads to the transformation of the heterostructure from a nontrivial topological state to a topological trivial state. The detailed orbital characters of bands near the Fermi level along Γ–Z–$H/4$ are exhibited in Fig. 3(e).

Third, the compressed lattice parameter under strain along the c-direction is increased to 2.4 Å ($\Delta c/c = -0.1644$). From Fig. 3, it can be seen that as compression progresses, not only is band I rapidly increasing, but also band III. Due to the lack of symmetry protection, band I splits between path Z–H. The orbit of band I splits into band IV dominated by p_z orbitals and band V dominated by (p_x, p_y) orbitals. Since the strain occurs only in the c-direction, the rate of rise in band V is much

higher than that in band V. Similarly, the band III splits into higher band VI dominated by p_z orbitals and lower band VII mixed with (p_x, p_y) orbitals. Because band VI rises faster than band V, they undergo band inversion between Z–H. In Fig. 3, the relevant electronic band structures indicate that band crossing occurs around TRIP Z in the plane $k_z = \pi$ above the Fermi level of 0.25 eV. The p_z orbital of atoms (Te1, Te2), p_y orbital of atom Te1 and p_z orbital of atom Bi are responsible for this band crossing, as displayed in Fig. 3(f). The energy gap induced by SOC is opened up to 50 meV, which means the possible existence of topological surface states. The calculation results of surface states also confirm our hypothesis. Thus, the van der Waals heterostructure BiTeCl/$HfTe_2$ under c-direction strain experiences topological phase transition twice. Within a certain range, if the heterostructure is further compressed, the topological properties of the material will remain unchanged. It is possible that a Dirac cone can be observed by an ARPES experiment involving the (110) surface.

To verify the topological properties under c-direction strain, we calculate topological invariants Z_2 and surface states for heterostructure BiTeCl/$HfTe_2$. In the case of compressed lattice parameter 1.2 Å, the topological nontrivial property can be tested by the Dirac cone surface state on the (110) surface as shown in Figs. 4(a) and 4(d). The Dirac cone is located at TRIP $\widetilde{Z}$ above Fermi level 0.15 eV. When the compressed lattice parameter is increased to 1.8 Å, the calculated topological invariant (0;000) indicates phase transition from nontrivial to trivial. This phenomenon is accompanied by the disappearance of the Dirac cone in Figs. 4(b) and 4(e). In the situation of compressed lattice parameter 2.4 Å, a new topological phase emerges with topological invariant (1;001). In Figs. 4(c) and 4(f), the corresponding topological surface state above the Fermi level 0.25 eV on the (110) surface is shown. Hence, heterostructure BiTeCl/$HfTe_2$ in these situations undergoes topological phase transition twice. The topological surface states can be tested directly by an ARPES experiment.

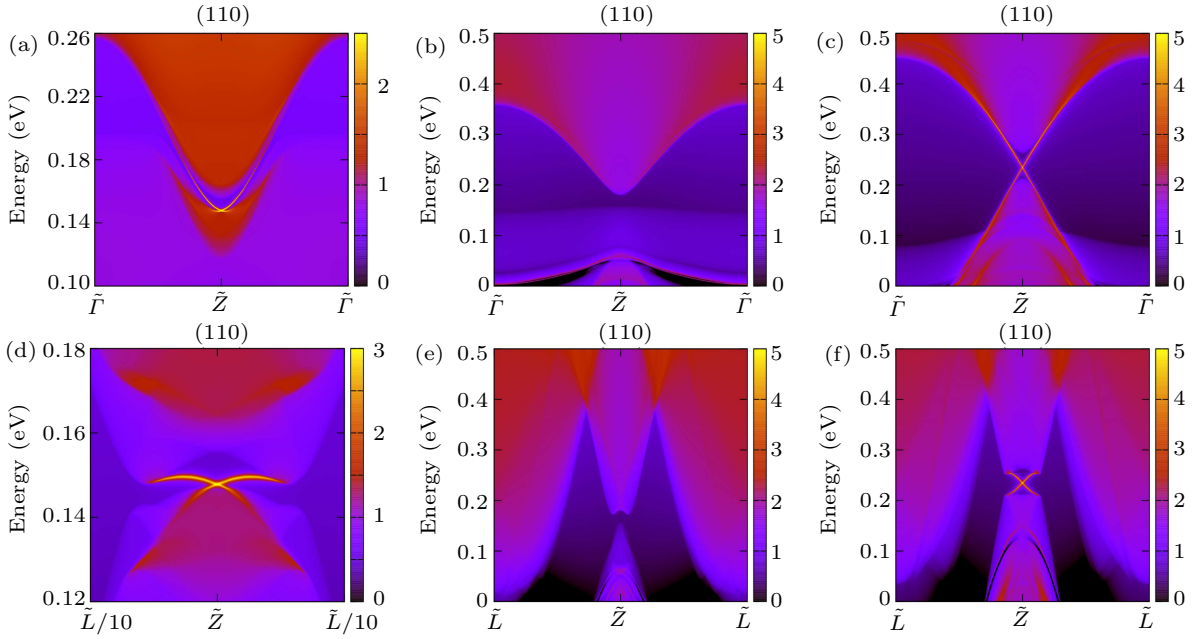


Fig. 4. The projected (110) surface states of heterostructure BiTeCl/$HfTe_2$ near the Fermi level at compressed lattice parameters 1.2 Å ($\Delta c/c = -0.0822$), 1.8 Å ($\Delta c/c = -0.1233$) and 2.4 Å ($\Delta c/c = -0.1644$) are shown in ((a), (d)), ((b), (e)) and ((c), (f)), respectively. Point $\widetilde{L}/10$ represents a point $|L$–$Z|/10$ away from point Z.

4. Discussion and conclusion

To realize topological superconductivity, we select 2D Ising superconductor $HfTe_2$ and layered material BiTeCl, which also exhibit superconductivity under pressure. Based on the construction of alternate layered $HfTe_2$ and BiTeCl, we find that nontrivial topological phase transitions are achieved by applying strains in the c-direction. Observable Dirac cones are found near 0.2 eV on (110) surfaces, which can be detected by ARPES experiments. The system has suffered phase transitions twice through different mechanisms of band inversion. The band inversion around TRIP Z between the p_z orbital of atoms (Te1, Bi) and the (p_x, p_y) orbitals of atom Te2 is responsible for the first nontrivial topology. With further strain strength, the second topological phase transition is caused by band crossing between the p_z orbital of atoms (Te1, Te2), the p_y orbital of atom Te1 and the p_z orbital of atom Bi. Hence, the nontrivial topology in layered heterostructure BiTeCl/$HfTe_2$ provides us with a new desirable platform upon which to construct topological superconductors.

References

[1] Zhang H J, Liu C X, Qi X L, Dai X, Fang Z and Zhang S C 2009 *Nat. Phys.* **5** 438

[2] Xia Y, Qian D, Hsieh D, Wray L, Pal A, Lin H, Bansil A, Grauer D, Hor Y S, Cava R J and Hasan M Z 2009 *Nat. Phys.* **5** 398

[3] Wang Z J, Sun Y, Chen X Q, Franchini C, Xu G, Weng H M, Dai X and Fang Z 2012 *Phys. Rev. B* **85** 195320
[4] Liu Z K, Zhou B, Zhang Y, Wang Z J, Weng H M, Prabhakaran D, Mo S K, Shen Z X, Fang Z and Dai X 2014 *Science* **343** 864
[5] Le C C, Qin S S, Wu X X, Dai X, Fu P Y, Fang C and Hu J P 2017 *Phys. Rev. B* **96** 115121
[6] Liu D F, Wei L Y, Le C C, Wang H Y, Zhang X, Kumar N, Shekhar C, Schröter N B M, Li Y W, Pei D and Chen Y L 2021 *J. Appl. Phys.* **129** 235109
[7] Li Y X, Le C C, Cheng Q B, Chen Y G and Chen B 2020 *Phys. Lett. A* **384** 126216
[8] Weng H M, Fang C, Fang Z, Bernevig B A and Dai Xi 2015 *Phys. Rev. X* **5** 011029
[9] Lv B Q, Weng H M, Fu B B, Wang X P, Miao Hu, Ma J Z, Richard P, Huang X C, Zhao L X, Chen G F and Ding H 2015 *Phys. Rev. X* **5** 031013
[10] Yu R, Fang Z, Dai X and Weng H M 2017 *Front. Phys.* **12** 127202
[11] Schindler F, Cook A M, Vergniory M G, Wang Z J, Parkin S S P, Bernevig B A and Neupert T 2018 *Sci. Adv* **4** eaat0346
[12] Sun H L, Huo M W, Hu X W, Li J Y, Liu Z J, Han Y F, Tang L Y, Mao Z Q, Yang P T, Wang B S and Wang M 2023 *Nature* **621** 493
[13] Kitaev A Y 2023 *Ann. Phys.* **303** 2
[14] Freedman M H 1998 *Proc. Natl. Acad. Sci. USA* **95** 98
[15] Fu L and Kane C L 2008 *Phys. Rev. Lett.* **100** 096407
[16] Luo A Y, Li Y, Qin Y, Hu J N, Wang X X, Zou J Y, Lian B and Xu Gang 2023 *npj Compu. Mater.* **9** 188
[17] Liu C J, Zhou X J, Hong D S, Fisher B, Zheng H, Pearson J, Jiang J D S, Jin D F, Norman M R and Bhattacharya A 2023 *Nat. Commun.* **14** 951
[18] Landolt G, Eremeev S V, Tereshchenko O E, Muff S, Slomski B, Kokh K A, Kobayashi M, Schmitt T, Strocov V N and Dil J H 2013 *New J. Phys.* **15** 085022
[19] Bahramy M S, Yang B J, Arita R and Nagaosa N 2012 *Nat. Commun.* **3** 679
[20] Ying J J, Struzhkin V V, Cao Z Y, Goncharov A F, Mao H K, Chen F, Chen X H, Gavriliuk A G and Chen X J 2016 *Phys. Rev. B* **93** 100504
[21] Momma K and Izumi F 2011 *J. Appl. Cryst.* **44** 1272
[22] Wang D W, Wu J Z and Si C 2023 *Nano Res.* **16** 11521
[23] Tsipas P, Pappas P, Symeonidou E, Fragkos S, Zacharaki C, Xenogiannopoulou E, Siannas N and Dimoulas A 2021 *APL Mater.* **9** 101103
[24] Wang C, Lian B, Guo X M, Mao J H, Zhang Z T, Zhang D, Gu B L, Xu Y and Duan W H 2019 *Phys. Rev. Lett.* **123** 126402
[25] Hajra D, Sailus R, Blei M, Yumigeta K, Shen Y X and Tongay S 2020 *ACS Nano* **14** 15626
[26] Chen Y L, Kanou M, Liu Z K, Zhang H J, Sobota J A, Leuenberger D, Mo S K, Zhou B, Yang S L, Kirchmann P S and Sasagawa T 2013 *Nat. Phys.* **9** 704
[27] Kresse G and Hafner J 1993 *Phys. Rev. B* **47** 558
[28] Kresse G and Furthmuller J 1996 *Comput. Mater. Sci.* **6** 15
[29] Kresse G and Furthmuller J 1996 *Phys. Rev. B* **54** 11169
[30] Gao X, Sun J, Wan X G and Li G 2022 *Chin. Phys. Lett.* **39** 077101
[31] Jin G, Lee C S, Okello O F N, Lee S H, Park M Y, Cha S, Seo S Y, Moon G and Jo M H 2021 *Nat. Nano* **16** 1092
[32] Zhao B, Wan Z, Liu Y, Xu J Q, Yang X D, Shen D Y, Zhang Z C, Guo C H, Qian Q, Li J and Duan X F 2021 *Nature* **591** 385
[33] Bai W, Hua Y, Nan P F, Dai S N, Sun L, Huang X L, Yang J, Ge B H, Xiao C and Xie Y 2023 *J. Am. Chem. Soc.* **146** 892
[34] Molina-Mendoza A J, Giovanelli E, Paz W S, Niño M A, Island J O, Evangeli C, Aballe L, Foerster M, Van Der Zant H S J and Rubio-Bollinger G 2017 *Nat. Commun.* **8** 14409
[35] Qin Y X, Li S S, Ji W X and Zhang C W 2024 *Chin. Phys. B* **33** 027901
[36] Perdew J P, Burke K and Ernzerhof M 1997 *Phys. Rev. Lett.* **77** 3865
[37] Monkhorst H J and Pack J D 1976 *Phys. Rev. B* **13** 5188
[38] Gresch D, Autes G, Yazyev O V, Troyer M, Vanderbilt D, Bernevig B A and Soluyanov A A 2024 *Phys. Rev. B* **95** 075146
[39] Medjanik K, Fedchenko O, Chernov S, Kutnyakhov D, Ellguth M, Oelsner A, Schönhense B, Peixoto T R F and Lutz P 2017 *Nat. Mater.* **16** 615
[40] Krizman G, Assaf B A, Phuphachong T, Bauer G, Springholz G, Bastard G, Ferreira R, De Vaulchier L A and Guldner Y 2018 *Phys. Rev. B* **98** 075303
[41] Wang H, Bang J H, Sun Y Y, Liang L B, West D, Meunier V and Zhang S B 2016 *Nat. Commun.* **7** 11504